Journal of Alloys and Compounds 509 (2011) 6561–6566

Contents lists available at ScienceDirect

Journal of Alloys and Compounds

journal homepage: www.elsevier.com/locate/jallcom

High tunability of pulsed laser deposited $Ba_{0.7}Sr_{0.3}TiO_3$ thin films on perovskite oxide electrode

R. Reshmi [a], A.S. Asha [a], P.S. Krishnaprasad [a], M.K. Jayaraj [a,*], M.T. Sebastian [b]

[a] Nanophotonic and Optoelectronic Devices Laboratory, Department of Physics, Cochin University of Science and Technology, Kochi, Kerala 682022, India
[b] National Institute of Interdisciplinary Science and Technology, Thiruvananthapuram, Kerala 695019, India

ARTICLE INFO

Article history:
Received 2 June 2010
Received in revised form 16 February 2011
Accepted 16 February 2011
Available online 9 March 2011

PACS:
81.15Fg
77.55.fe
73.50.−h

Keywords:
Pulsed laser deposition
Ferroelectrics

ABSTRACT

Ferroelectric thin films such as BST, PZT and PLZT are extensively being studied for the fabrication of DRAMS since they have high dielectric constant. The large and reversible remnant polarization of these materials makes it attractive for nonvolatile ferroelectric RAM application. In this paper we report the characterization of $Ba_{0.7}Sr_{0.3}TiO_3$ (BST) thin films grown by pulsed laser ablation on oxide electrodes. The structural and electrical properties of the fabricated devices were studied. Growth of crystalline BST films was observed on $La_{0.5}Sr_{0.5}CoO_3$ (LSCO) thin film electrodes at relatively low substrate temperature compared to BST grown on PtSi substrates. Electrical characterization was carried out by fabricating PtSi/LSCO/BST/LSCO heterostructures. The leakage current of the heterostructure is studied and a band structure is modeled based on the transport properties of the heterostructure. The dielectric constant of the BST film is found to be 630 at 100 kHz with a loss tangent of 0.04. The capacitance voltage characteristics show high tunability for BST thin films.

1. Introduction

Ferroelectric oxide thin films with perovskite structure are of great technological interest. The tunable devices such as varactors, filters, oscillators, and phase shifters make use of the nonlinearity of the internal electrical polarization, of ferroelectric materials, steerable by an external electric field [1–4]. Compared to the popular tuning elements such as p–i–n diodes, GaAs Schottky diodes or ferromagnetics, ferroelectric components offer the advantages of continuous, quick, low power tunability up to gigahertz frequencies [5,6].

Barium strontium titanate ($Ba_xSr_{(1-x)}TiO_3$) (BST), an environment friendly lead-free ferroelectric material, is an attractive candidate for microelectronic devices and optoelectronic applications. The perovskite thin film of (Ba,Sr)TiO_3 (BST) exhibits high relative dielectric constant, low dielectric dissipation factor, low leakage current, and strong tunability under an external dc electric field. BST can be integrated to the existing semiconductor processing technology for next generation of gigabyte dynamic random access memories (DRAMs), microwave tunable devices, field effect transistors (FETs), and electrooptic devices [7–13].

For the ABO_3 perovskite, different A site and B site dopants (where A = Ca, Sr, La; B = Nb, Ta, Zr) are used to modify the electrical properties of $BaTiO_3$ based compositions [1–3,14]. $Ba_xSr_{(1-x)}TiO_3$ is the solid solution between barium titanate ($BaTiO_3$) and strontium titanate ($SrTiO_3$) and can be formed in the entire range of composition. The dielectric and ferroelectric properties of $Ba_xSr_{(1-x)}TiO_3$ depend on Sr content. At room temperature $Ba_xSr_{(1-x)}TiO_3$ is ferroelectric, for low Sr content, that is x is in the range of 0.7–1 and is paraelectric when x is in the range 0–0.7 [15]. As a result the electrical and optical properties of BST can be tailored over a broad range for various electronic applications [16].

Ferroelectric thin films have been successfully deposited by rf sputtering [17–19], metal organic chemical vapor deposition [17], sol gel [8,9,12,17] and pulsed laser deposition (PLD) [7,17,20–24]. Among these processes the PLD technique is superior since it possesses the advantages viz., lower synthesis temperature, easy to control the stoichiometry of thin films, possibility of depositing oxides of high melting point and materials of metastable phase [17].

Leakage current characteristics of BST films are influenced by the electrode and film electrode interface characteristics. Deposition conditions, composition and electrode structure play the most significant role in leakage current characteristics. Understanding the current transport mechanism is crucial and most of the knowledge is based on the transport across the interfacial potential barrier at the cathode when thermoionic emission, thermoionic field emission, or a combination of these is dominant. The leakage current

* Corresponding author. Tel.: +91 484 2577404.
E-mail address: mkj@cusat.ac.in (M.K. Jayaraj).

0925-8388/$ – see front matter © 2011 Elsevier B.V. All rights reserved.
doi:10.1016/j.jallcom.2011.02.074

density J increases with increasing temperature leading to the increased probability for the electrons to overcome or to tunnel the barrier either at the interface or in the bulk due to higher thermal energy [25].

The oxygen vacancies play an important role in perovskite ferroelectrics. Though the oxygen ambient is used to prevent the formation of oxygen vacancies in the deposited film, it has been shown that oxide films grown using PLD at high oxygen ambient pressure are still oxygen deficient [21,22,26,27]. The lattice of an O_2 deficient BST film expands beyond the size than that for the corresponding bulk ceramics [22,26,27]. One of the main technological challenges is to find a suitable electrode material with low electrical resistivity, good thermal stability, high resistance to oxidation and good adhesion both to substrate and the ferroelectric film. The interfacial defect layers may originate from accumulation of oxygen vacancies. Under the electric field oxygen vacancies migrate towards the electrode and aggregate near the electrode interface. The use of conducting oxide electrodes or aqueous solution electrodes helps to compensate the oxygen vacancies in the electrode–film interface [28] thereby inhibiting the accumulation of oxygen vacancies at the interface. As a result no interfacial defect layer is formed at ferroelectric–electrode interface [28]. Perovskite conducting oxide $La_{0.5}Sr_{0.5}CoO_3$ (LSCO) is obtained from ABO_3 perovskite $LaCoO_3$ by partial substitution of La^{3+} by Sr^{2+} [29,30]. The crystal structure of LSCO is same as that of the perovskite ferroelectrics which makes it a potential candidate as electrode for ferroelectric memory devices. The LSCO which is a conductive oxide electrode act as oxygen vacancy sink for the BST capacitors thereby reducing the fatigue problem usually encountered while using conventional platinum electrode [7,31–35]. The similar crystal structure of LSCO and perovskite ferroelectrics facilitates the easy growth of ferroelectrics over textured or epitaxially grown LSCO layer [36,37].

Some problems of porosity and poor adhesion are often reported for BST films and very high temperature thermal treatment is generally required to achieve well-crystallized BST films. Such a high temperature process could limit drastically the application of these BST films in integrated circuits [5,16]. A low processing temperature is crucial for application of these thin film materials in integrated electronic devices. With an oxide buffer or electrode layer the deposition temperature can be reduced.

In this paper we report the study of the growth of ferroelectric (BST) $Ba_{0.7}Sr_{0.3}TiO_3$ films on $La_{0.5}Sr_{0.5}CoO_3$ (LSCO) oxide electrode at relatively low temperature without any post deposition heat treatment. The electrical properties of the PtSi/LSCO/BST/LSCO structure were carried out and a band structure is proposed to explain the leakage current mechanisms. The multilayer oxide structure exhibits ferroelectric nature with a good remnant polarization and low coercive field.

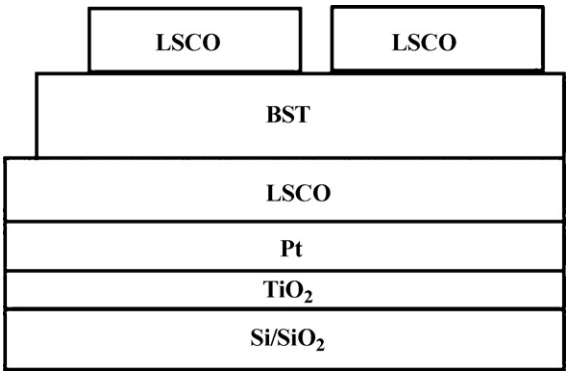

Fig. 1. Schematic diagram of the heterostructure used in the study.

2. Experimental

The target for PLD was prepared by solid state reaction of barium titanate ($BaTiO_3$) and strontium titanate ($SrTiO_3$). The mixture was pressed and sintered at 1450 °C for 5 h to obtain $Ba_{0.7}Sr_{0.3}TiO_3$ (BST). The fourth harmonics of Q-switched Nd:YAG laser (266 nm) was used for ablation. The repetition frequency was 10 Hz with a pulse width of 6–7 ns. The laser fluence was kept at 2 J/cm^2. The target to substrate distance was kept at 3.5 cm. The substrate temperature (T_s) was kept at 500 °C and oxygen partial pressure in the chamber was maintained at 0.15 mbar.

The crystallinity of thin films was determined by X-ray diffraction (XRD, Rigaku DMax – C) with CuKα radiation (λ = 1.541 Å). The surface morphology was analysed by scanning electron microscope (SEM, JEOL JSM 5600). The composition was analysed using energy dispersive X-ray (EDX; JEOL JSM 5600). Thickness of the films was measured using Dektak 6M surface profiler. Electrical characterization was carried out using Keithly source measure unit SMU236. The dielectric constant was calculated from the capacitance measured with LCR meter (HP-4192A) by sweeping the voltage as well as the frequency.

Commercial Si/SiO_2/Pt wafers were used as the substrate for deposition. The structure of discrete capacitors is shown in Fig. 1. Both the top and bottom LSCO electrodes were deposited by rf magnetron sputtering. The sputtering power was kept at 100 W with an argon gas pressure of 0.003 mbar at 600 °C. The films were crystalline and had a thickness of about 400 nm. The resistivity of all the samples was of the order 10^{-5} Ω cm. The growth and characterization of LSCO thin films has been reported elsewhere [38].

3. Results and discussion

3.1. Structural and compositional analysis

The crystallinity of BST thin films deposited at substrate temperature of 500 °C and at a pressure of 0.15 mbar have been studied by X-ray diffraction. The XRD pattern of the heterostructure PtSi/LSCO/BST/LSCO is shown in Fig. 2a. The BST perovskite film was

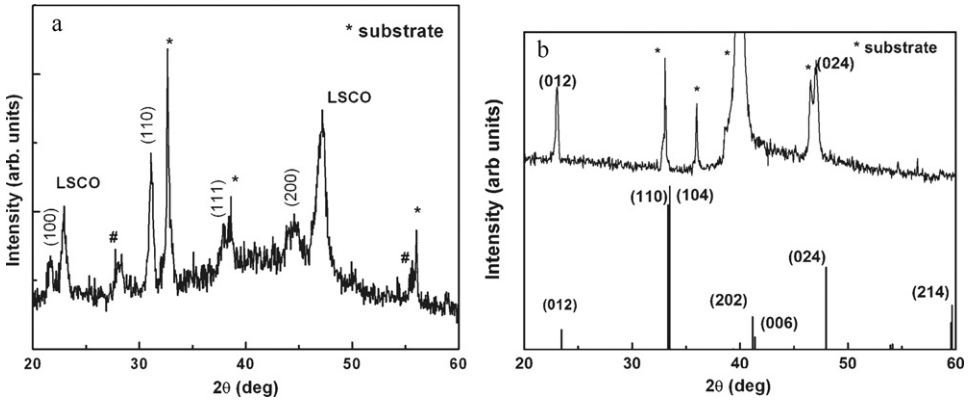

Fig. 2. (a) The XRD pattern of PtSi/LSCO/BST/LSCO grown at 500 °C at 0.15 mbar (# represents pyrochlore phases of BST). (b) The XRD pattern of PtSi/LSCO deposited by rf sputtering.

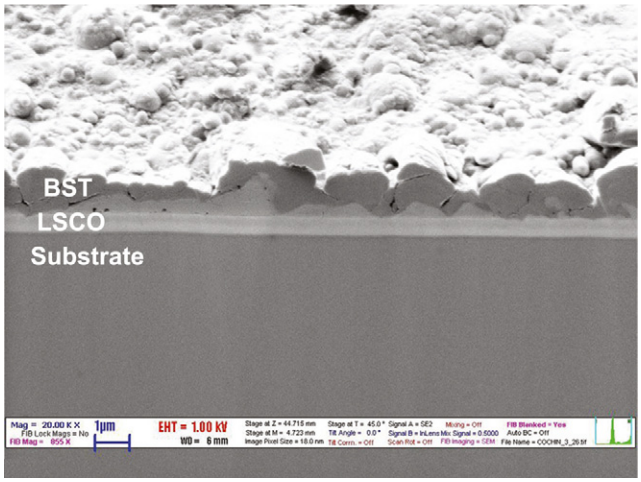

Fig. 3. Cross sectional SEM image of PtSi/LSCO/BST.

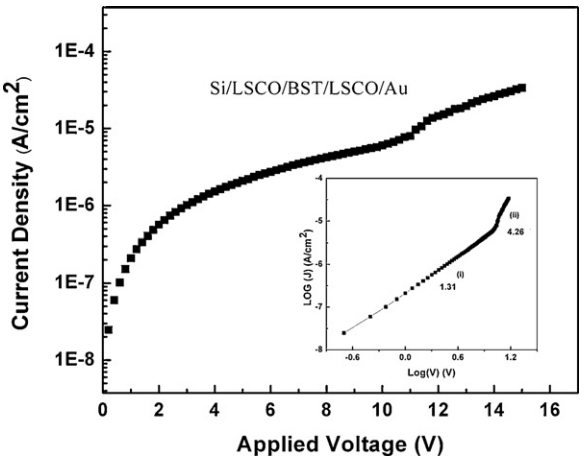

Fig. 4. The room temperature leakage current for the device PtSi/LSCO/BST/LSCO. Variation of log J as a function of log V for PtSi/LSCO/BST/LSCO(inset).

grown at a lower substrate temperature on the LSCO electrodes. These oxide electrodes act both as a template and as electrode for BST thin films. The lattice constants of BST and LSCO films are calculated from their respective XRD pattern. The perovskite BST thin film has a lattice constant of 3.95 Å. The LSCO material has perovskite structure with lattice parameter $a = 3.805$ Å. Crystalline growth of BST on LSCO thin films is due to the same crystal structure, lattice parameter and atomic arrangements of LSCO layer and BST layer [39]. Fig. 2b shows the pure perovskite phase formation of LSCO on PtSi substrate. The BST films deposited on PtSi under the same condition as that of device was also phase pure. During the device fabrication, the growth of BST films on LSCO electrode may have resulted in the formation of pyrochlore phases in BST. The cross sectional SEM of the samples shown in Fig. 3 reveals that the interface between the LSCO and BST layer is sharp. The compositional analysis of thin films carried out using EDX shows that the films with perovskite phase has Ba + Sr/Ti ratio approximately 1.

3.2. Electrical characterization

The leakage current of the samples was found from the current–voltage (I–V) curve. The leakage current is an important characteristic of thin film ferroelectric capacitors, it directly limits the charge retention and it influences the ferroelectric hysteresis loop. The leakage current is also a sensitive electrical probe of the material quality of heterostructure as it is strongly dependent on material aspects of the ferroelectric film and of electrode–ferroelectric interfaces [40]. Capacitor with low leakage current is ideal for microelectronic device application.

The current density vs. electric field characteristics of the BST capacitor for the structure PtSi/LSCO/BST/LSCO are shown in Fig. 4. The leakage current density of BST thin film capacitor with LSCO electrode is found to be 200 nA/cm^2 at a bias voltage of 2 V for 800 nm thick BST film. The low leakage current density of the capacitor with LSCO electrode makes it a potential candidate for gigabit density memories [41].

log J vs. log V plots of the capacitor shown in the inset of Fig. 4 reveals the leakage current mechanism in the low voltage region. In the low voltage regime the graph is linear with a slope of 1.31. The contact LSCO/BST can be considered to be ohmic like under low field strength. At high voltage the distribution of electrons between LSCO and BST can be disturbed and the leakage current deviates from ohmic behavior. In the high voltage region the conduction mechanism is dominated by Pool Frenkel mechanism. To ensure that the conduction mechanism is Pool Frenkel, the data in Fig. 4 is replotted as log(J/E) vs. $\sqrt{V}$ as shown in Fig. 5. The log(J/E) curve shows small increase with $\sqrt{V}$ in the low voltage region. At high voltage the value increases linearly with $\sqrt{V}$.

The variation of log J with measured voltage as a function of temperature is shown in Fig. 6. The variation of log(J/E) with 1000/T for various voltages is plotted. All the films showed good linearities with negative slopes suggesting thermally activated leakage current mechanism. A typical plot is shown in Fig. 6b. Activation energy measures the thermal energy required to raise electrons from the donor level to the conduction band. The oxygen vacancies in BST thin films create donor levels. Hence as temperature increases the electrons from the donor levels are excited to the conduction band. This will result in an increase of current through the heterostructure.

The activation energies at each voltage are calculated from the slopes of each plot. The activation energy as a function of $\sqrt{V}$ is plotted in Fig. 7. This figure shows the two different leakage current mechanism operating in the high and low voltage regions. In the high voltage region the activation energies decrease in a linear fashion with $\sqrt{V}$ with larger absolute values than those in the low voltage regions. Mean squared linear fitting for the high voltage region when extrapolated to $V = 0$ gives the activation energy at $V = 0$ as 1.3 eV.

In the low voltage region the linear decrease in activation energy with square root of the applied voltage suggests that the conduction is not purely ohmic but rather a type of field enhanced thermally

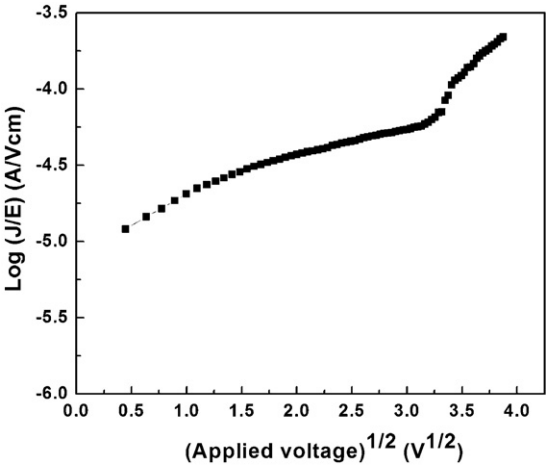

Fig. 5. Variation of log J/E as a function of $\sqrt{V}$ for the device PtSi/LSCO/BST/LSCO.

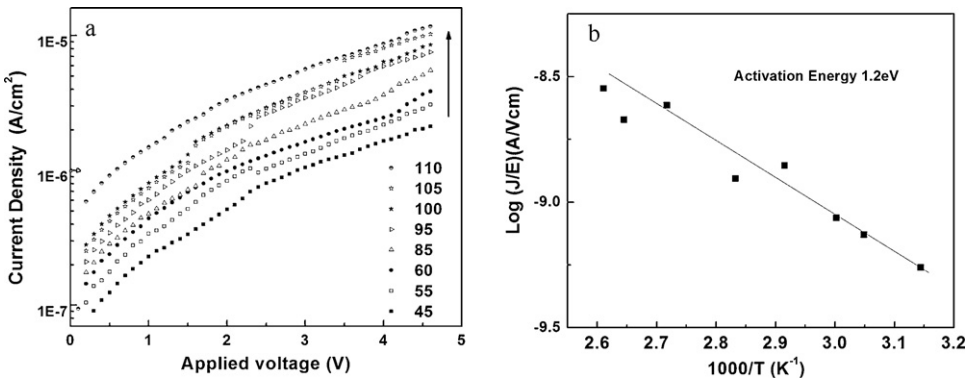

Fig. 6. (a) Variation of log$J$ as a function of voltage at various temperature for the device PtSi/LSCO/BST/LSCO (arrow indicates the increasing order of temperature in °C). (b) The variation of logJ/E as a function of 1000/T for the device PtSi/LSCO/BST/LSCO.

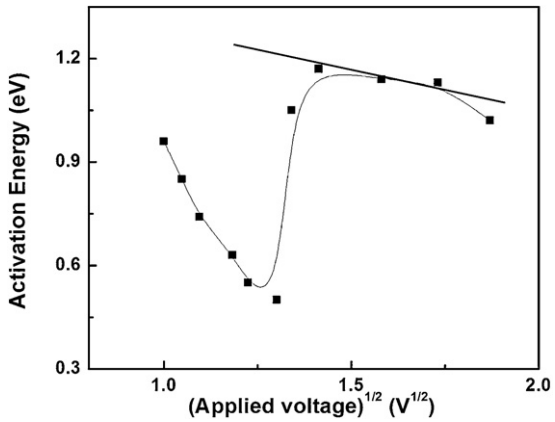

Fig. 7. Variation of the activation energy for the device PtSi/LSCO/BST/LSCO as a function of $\sqrt{V}$.

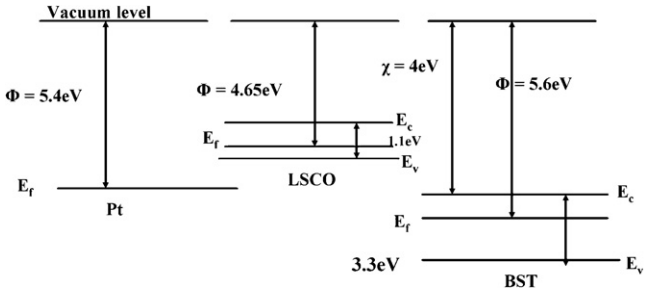

Fig. 8. Energy band diagram for the device PtSi/LSCO/BST/LSCO.

activated process is involved. This may be the reason for the slope being larger than 1 in the log$J$-log$V$ plot (inset of Fig. 4). At high voltage region the leakage current deviates from ohmic or ohmic like behavior. The activation energy in the high voltage region decreases linearly with $\sqrt{V}$ suggesting that a field enhanced thermally activated process is responsible for electrical conduction in this region. The slopes of the plot log$J$–log$V$ and that obtained by extrapolation of activation energy to $V = 0$ are the same. Therefore at high voltages the electrical conduction mechanism can be attributed to Pool Frenkel emission.

A band structure based on the conduction mechanism is proposed in the present study. The ohmic nature of LSCO/BST implies that the surface states of the BST in contact with LSCO are different from that with metal electrode. The main difference is in the nature of chemical bonding of BST with oxide electrode. The oxygen ions in the LSCO strongly interact with oxygen and cations in the BST thus forming chemical bonds. In the case of metal/BST the chemical states of the surface dangling bonds can be preserved after contact formation but on LSCO/BST most of the dangling bonds disappear due to the interaction of oxide electrode with BST [42]. The contact between BST and LSCO is ohmic as observed in Fig. 4. The oxygen vacancy concentration is reduced and the Fermi level is located closer to the center of the energy band. The LSCO can release oxygen to the oxygen deficient BST during the film formation. Fig. 8 shows the schematic energy bands for PtSi/LSCO/BST/LSCO devices.

The dielectric constant of the heterostructure PtSi/LSCO/BST/LSCO is calculated using the relation

$$C = \frac{A\varepsilon\varepsilon_r}{d} \quad (1)$$

where C is the measured capacitance in Farads, ε the free space dielectric constant (8.85×10^{-12} F/m), A the area of the capacitor (m^2) and d (m) the thickness of the ferroelectric thin film.

PtSi/LSCO/BST/LSCO showed appreciable capacitance with minimum loss. The variation of dielectric constant measured with PtSi/LSCO/BST/LSCO capacitor configuration with BST film grown by PLD is shown in Fig. 9. The dielectric constant of the crystallized films was found to be about 630 and the loss tangent about 0.04 at a frequency of 100 kHz. The relatively slight increase in the loss factor may be due to the high surface roughness of the film. As compared to bulk values the dielectric constant of thin films was found to be low, which is a consequence of the small grain size of the grown films. The dielectric constant and the loss factor showed no noticeable dispersion with frequency, indicating good quality of the film and the absence of internal interfacial barriers [37]. However

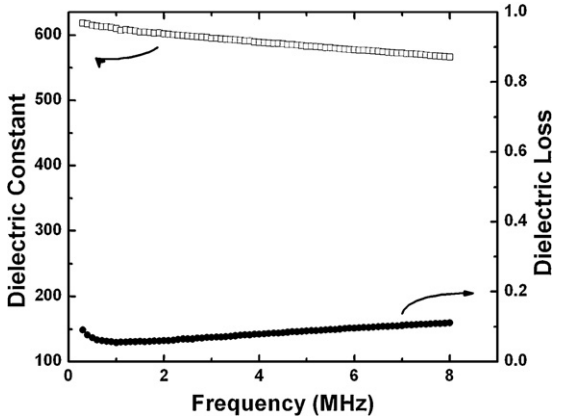

Fig. 9. The variation of dielectric constant and loss with frequency for PtSi/LSCO/BST/LSCO.

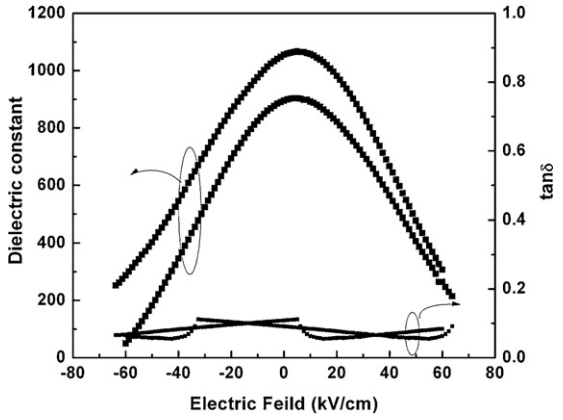

Fig. 10. Variation of dielectric constant and dielectric loss of PtSi/LSCO/BST/LSCO structure measured at 1 kHz.

it can be seen from the figure that there is a slight decrease in the dielectric constant with increase in frequency, which suggests that at higher frequency the contribution from possible dc conduction decreases.

The charge–voltage characteristics of the BST thin films with oxide electrode in the configuration PtSi/LSCO/BST/LSCO is studied. Fig. 10 shows the room temperature dielectric constant ε and loss tangent $\tan\delta$ as a function of the applied dc electric field where the relative dielectric constant ε_r was calculated from the capacitance data using the classical formula of parallel-plate capacitors. The capacitance–voltage characteristics of the BST films were measured at a frequency of 1 kHz. The dielectric properties of BST thin films are highly tunable through the application dc bias field.

The tunability is defined as the

$$\text{tunability} = \frac{[\varepsilon(0) - \varepsilon(E)]}{\varepsilon(0)} \times 100\% \quad (2)$$

where $\varepsilon(0)$ and $\varepsilon(E)$ are the dielectric constant at zero field and at an applied field E, respectively. The figure of merit (K) is given by

$$K = \frac{\%\text{tunability}}{\tan\ \delta} \quad (3)$$

The variation of tunability and figure of merit with the dc field is shown in Fig. 11. The films show high tunability and good figure of merit with oxide electrodes. High value of tunability can be attributed to the better growth of BST thin films on oxide electrode.

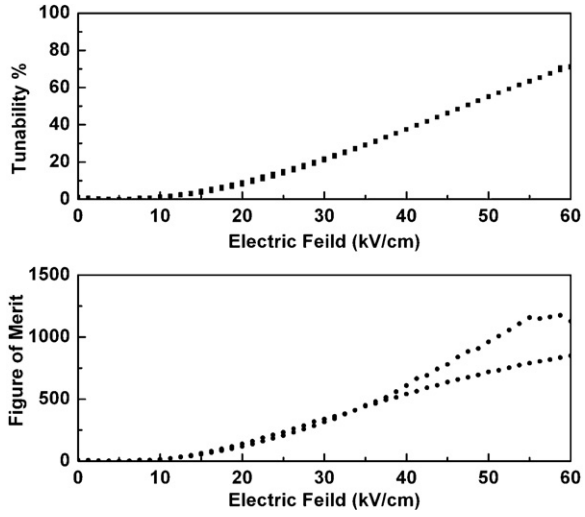

Fig. 11. Variation of tunability and figure of merit of PtSi/LSCO/BST/LSCO structure with dc bias voltage.

4. Conclusions

BST thin films deposited on LSCO, an oxide perovskite electrode, were found to be crystalline at relatively low substrate temperature without any post deposition heat treatment. The LSCO serves as a template as well as bottom electrode for the BST thin film capacitors. The interface between the oxide electrode and the BST layer is sharp and free from defects. The dielectric constant of BST is studied as a function of frequency. The devices showed little dispersion with frequency. The loss was found to be minimum for films deposited on oxide template. The study of leakage current shows that the films are insulating. Based on the transport properties a band structure has been proposed. The films showed ohmic nature at low field and a Pool Frenkel emission at high fields with an electron trapping energy of 1.3 eV. The capacitance voltage characteristics show high tunability with low dielectric loss. The figure of merit for the structure is also high making BST thin films a promising material for frequency agile application.

Acknowledgment

This work is supported by Department of Science and Technology, Government of India.

References

[1] H. Tian, Y. Wang, J. Miao, H. Chan, C. Choy, J. Alloys Compd. 431 (2007) 197.
[2] J. Chen, Y. Tseng, C. Huang, J. Alloys Compd. 494 (2010) 205.
[3] F. Boujelben, F. Bahri, C. Bouday, A. Maalej, H. Khemakhem, A. Simon, M. Maglione, J. Alloys Compd. 481 (2009) 551.
[4] Z. Hu, Y. Li, M. Zhu, Z. Zhu, J. Chu, Phys. Lett. A 372 (2008) 4521.
[5] X.H. Zhu, B. Guigues, E. Defaÿ, C. Dubarry, M. Aïd, J. Appl. Phys. 105 (2009) 44108.
[6] A.K. Tagantsev, V.O. Sherman, K.F. Astafiev, J. Venkatesh, N. Setter, J. Electroceram. 11 (2003) 5.
[7] L. López, J. Portelles, J. Siqueiros, G. Hirata, J. McKittrickb, Thin Solid Films 373 (2000) 49.
[8] S.U. Adikary, H. Chan, Thin Solid Films 424 (2003) 70.
[9] M. Cernea, E. Andronescu, R. Radu, F. Fochi, C. Galassi, J. Alloys Compd. 490 (2010) 690.
[10] O. Auciello, S. Saha, D.Y. Kaufman, S.K. Streiffer, W. Fan, B. Kabius, J. Im, P. Baumann, J. Electroceram. 12 (2004) 119.
[11] M.W. Cole, W.D. Nothwang, J.D. Demaree, S. Hirsch, J. Appl. Phys. 98 (2005) 24507.
[12] W. Li, Z. Xu, R. Chu, P. Fu, J. Hao, J. Alloys Compd. 499 (2010) 255.
[13] Y. Wang, B. Liu, F. Wei, Z. Yang, J. Du, J. Alloys Compd. 475 (2009) 827.
[14] Q. Xu, X. Zhang, Y. Huang, W. Chen, H. Liu, M. Chen, B. Kim, J. Alloys Compd. 488 (2009) 448.
[15] B.A. Baumert, L.H. Chang, A. Mastuda, T.L. Tsai, C. Tracy, R. Gregory, P. Fejas, N. Caves, J. Appl. Phys. 82 (1997) 2558.
[16] E. Ngo, P.C. Joshi, M.W. Cole, C.W. Hubbard, Appl. Phys. Lett. 79 (2001) 248.
[17] K.P. Jayadevan, T.Y. Tseng, J. Mater Sci.: Mater. Electron. 13 (2002) 439.
[18] Y.D. Xia, D. Wu, Z.G. Liu, J. Phys. D 37 (2004) 2256.
[19] Z. Feng, W. Chen, O.K. Tan, Mater. Res. Bull. 44 (2009) 1709.
[20] D. Roy, S.B. Krupanidhi, Appl. Phys. Lett. 62 (1993) 1056.
[21] L.A. Knaus, J.M. Pond, J.S. Horwitz, D.M. Chrisey, C.H. Mueller, R. Treece, Appl. Phys. Lett. 69 (1996) 25.
[22] E.J. Tarsa, E.A. Hachfield, F.T. Quinlan, J.S. Speck, M. Eddy, Appl. Phys. Lett. 68 (1996) 490.
[23] W. Hana, X. Chen, E. Xie, Mater. Res. Bull. 463 (2008) 25.
[24] N. Chan, G. Gao, Y. Wang, H. Chan, Thin Solid Films 518 (2010) e82.
[25] B. Panda, A. Roy, A. Dhar, S.K. Ray, J. Appl. Phys. 101 (2007) 64116.
[26] S.T. Lee, N. Fujimura, T. Ito, Jpn. J. Appl. Phys. 1 (34) (1995) 5168.
[27] W.J. Kim, W. Chang, S.B. Qadri, J.M. Pond, S.W. Kirchoefer, J.S. Horwitz, D.B. Chrisey, Appl. Phys. A: Mater. Sci. Process. 70 (2000) 313.
[28] H.Z. Jim, J. Zhu, J. Appl. Phys. 92 (2002) 4594.
[29] S. Saha, S.B. Krupanidhi, Mater. Sci. Eng. B 57 (1999) 135.
[30] C.J. Peng, S.B. Krupanidhi, Thin Solid Films 144 (1997) 305.
[31] G.W. Dietz, M. Schumacher, R. Waser, S.K. Streiffer, C. Basceri, A.I. Kingon, J. Appl. Phys. 82 (1997) 2359.
[32] V.E. Henrich, G. Dresselhaus, R.J. Zeiger, Phys. Rev. B 17 (1988) 4908.
[33] L. Hafid, G. Godefroy, A. Idrissi, F. Michel-Calendini, Solid State Commun. 66 (1988) 841.
[34] C.J. Peng, S.B. Krupanidhi, J. Mater. Res. 10 (1995) 708.

[35] H.Z. Jin, J. Zhu, P. Ehrhart, F. Fitsilis, C.L. Jia, S. Regnery, K. Urban, R. Waser, Thin Solid Films 429 (2003) 282.
[36] J.G. Simmons, Phys. Rev. 166 (1968) 912.
[37] M. Sayer, A. Mansigh, A.K. Arora, A. Lo, Integr. Ferroelectr. 1 (1992) 129.
[38] A.S. Asha, M.K. Jayaraj, M.T. Sebastian, J. Alloys Compd. 68 (2008) 449.
[39] M.H. Yeh, K.S. Liu, I.N. Lin, J. Mater. Res. 9 (1994) 2379.
[40] M. Dawber, K.M. Rabe, J.F. Scott, Rev. Mod. Phys. 77 (2005) 1083.
[41] B. Nagaraj, T. Sawhney, S. Perusse, S. Aggarwal, R. Ramesh, V.S. Kaushik, S. Zafar, R.E. Jones, J.H. Lee, V. Balu, J. Lee, J. Appl. Phys. 74 (1999) 3194.
[42] C.S. Hwang, B.T. Lee, C.S. Kang, J.W. Kim, K.H. Lee, H.J. Cho, H. Horii, W.D. Kim, S.I. Lee, Y.B. Roh, M.Y. Lee, J. Appl. Phys. 83 (1998) 3703.